ACSNANO

www.acsnano.org

ARTICLE

Morphology and Pattern Control of Diphenylalanine Self-Assembly *via* Evaporative Dewetting

Jiarui Chen,[†] Shuyu Qin,[†] Xinglong Wu,*[,†] and and Paul K. Chu[‡]

[†]Key Laboratory of Modern Acoustics, MOE, Institute of Acoustics and Collaborative Innovation Center of Advanced Microstructures, National Laboratory of Solid State Microstructures, Nanjing University, Nanjing 210093, P. R. China

[‡]Department of Physics and Materials Science, City University of Hong Kong, Tat Chee Avenue, Kowloon, Hong Kong, China

Supporting Information

ABSTRACT: **Self-assembled peptide nanostructures have unique physical and biological properties and promising applications in electrical devices and functional molecular recognition. Although solution-based peptide molecules can self-assemble into different morphologies, it is challenging to control the self-assembly process. Herein, controllable self-assembly of diphenylalanine (FF) in an evaporative dewetting solution is reported. The fluid mechanical dimensionless numbers, namely Rayleigh, Marangoni, and capillary numbers, are introduced to control the interaction between the solution and FF molecules in the self-assembly process. The difference in the film thickness reflects the effects of Rayleigh and Marangoni convection, and the water vapor flow rate reveals the role of viscous fingering in the emergence of aligned FF flakes. By employing dewetting, various FF self-assembled patterns, like concentric and spokelike, and morphologies, like strips and hexagonal tubes/rods, can be produced, and there are no significant lattice structural changes in the FF nanostructures.**

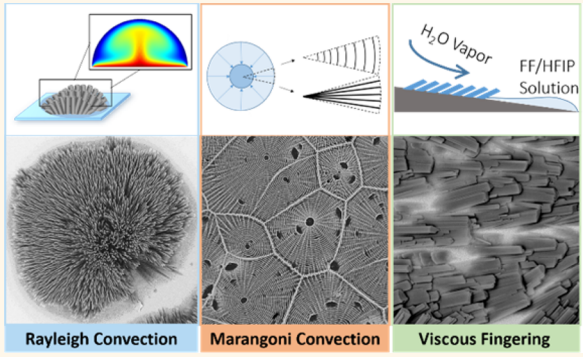

KEYWORDS: *diphenylalanine self-assembly, evaporative dewetting, morphology and pattern control*

Among the various types of materials for self-assembly, diphenylalanine (FF), the core recognition motif of the Alzheimer's β-amyloid polypeptide,[1] possessing unique properties such as morphological diversity,[2] facile synthesis,[1] and multifunctionality[3,4] has many potential applications in energy devices,[5] biosensors,[6] catalysts,[7] and photonics.[8] Although the interactions between FF molecules such as hydrogen bond, hydrophobic interaction, $\pi-\pi$ stacking, and electrostatic force have been investigated experimentally and theoretically,[9−12] it is still difficult to arrange FF components hierarchically into the desired structures and patterns.[11,13] Hence, it is technologically and scientifically important to clarify the self-assembly mechanism in order to produce the desirable hierarchical FF architecture in a controllable manner.

The dewetting phenomenon in which a thin liquid film on a substrate ruptures into droplets is common in nature.[14,15] Typical examples are the "coffee ring" effect[16,17] and "tears of wine",[18] and the underlying fluid mechanical effects have been considered in the formation of complexes or regular patterns of inorganic and organic nanoparticles.[19−21] If a certain amount of FF is dissolved in 1,1,1,3,3,3-hexafluoro-2-propanol (HFIP) or another volatile solvent and undergoes ultrasonic treatment to prevent premature aggregation (Figure 1a)[1,22,23] and the FF/HFIP solution is spread on the substrate in a humid environment (Figure 1b), self-assembled structures with unique morphologies or patterns emerge after the solution dries (Figure 1c−e). As shown by Reches and Gazit,[23] vertically grown FF nanotubes can be produced by dehydrating the FF−HFIP solution on the SiO_2 substrate (Figure 1c). The possible mechanism is that evaporation induces stacking of the FF monomers toward the liquid−air interface. Hendler *et al.*[24] have reported organized films consisting of spokelike FF nanotubes produced by heat treatment of FF nanotubes and *N*-methyl-2-pyrrolidone (Figure 1d). Control of the evaporation parameters such as the FF nanotube concentration, temperature, and environmental conditions are crucial to material growth. Spherulitic recrystallization is considered as a possible film formation mechanism. Ryu and Park have produced aligned FF nanorods from a thin solid FF film (Figure 1e).[25] These nanorods form under flowing H_2O vapor but fade under HFIP

Received: September 21, 2015
Accepted: December 11, 2015

DOI: 10.1021/acsnano.5b05936
ACS Nano XXXX, XXX, XXX−XXX

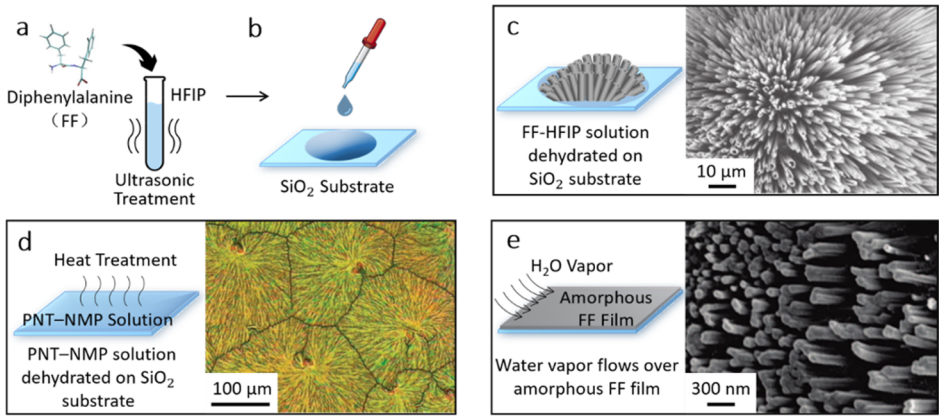

Figure 1. Schematic illustration of the typical experimental procedures to produce the FF structures: (a) Lyophilized FF powders are dissolved in the HFIP solvent under sonication; (b) A drop of the FF/HFIP solvent is deposited on the SiO_2 substrate; (c) Schematic (left) and SEM image (right) of the vertically aligned FF nanotubes reported by Reches and Gazit (ref 23.); (d) Schematic of the preparation process (left) and optical image (right) of the organized peptide nanotube film reported by Hendler *et al.* (ref 24.); (e) Schematic of the preparation process (left) and SEM image (right) of the aligned peptide nanorods reported by Ryu and Park (ref 25.).

vapor flow. The limitation of the solid FF film on mass transport has been suggested to be responsible for the structure formation. Other structures like vesicles,[10] tubes,[26,27] rods,[22] and wires[28,29] have been selectively produced by controlling factors such as the temperature,[30] sonication time,[22] relative humidity,[2] pH,[31] and solvent types.[32] Recently, it has been demonstrated that the FF and Fc–FF (ferrocene–FF) moieties can hierarchically coassemble into a dandelion-like structure driven *via* capillary force.[33] Although these self-assembling processes take place under different conditions, there is evidence that FF self-assembly depends on the interaction between FF molecules and fluid mechanical effects which have not been considered previously. It is possible to achieve effective control of the FF self-assembled morphologies and patterns by considering three major hydrodynamic effects, namely Rayleigh and Marangoni convection and the viscous fingering effect occurring in dewetting.

RESULTS AND DISCUSSION

In most cases, FF self-assembly occurs in a volatile solution (usually HFIP or HFIP/water or in a mixture with two miscible solvents).[32] To understand how an unstable solution affects FF self-assembly and avoid processes involving complicated solvents, we consider the case in which the FF/HFIP solution dewets on a substrate by evaporation in the subsequent steps (Figure 1b). The three major fluid mechanical effects in evaporative dewetting are heat-transferring Rayleigh convection caused by buoyancy force,[34] Marangoni convection by surface tension,[19,35] and viscous fingering by the viscosity difference in the phase boundary.[36] To investigate the role of each individual effect, the FF/HFIP solution deposited on a horizontal substrate is assumed to be an incompressible liquid film with a rigid, conductive lower surface and a free, flat upper surface. A linear temperature gradient is imposed normal to the upper surface to introduce instability to the film (Figure 2a). The unique FF structures and patterns usually formed in unstable solutions are dominated by different effects.[37,38] Therefore, factors that characterize the change in the solution stability are of interest. Thermophysical quantities such as the liquid density ρ, surface tension δ, and dynamic viscosity μ are assumed to be constant for simplicity, and the definitions of Rayleigh number (Ra) and Marangoni number (Ma) are given in Table S1. In

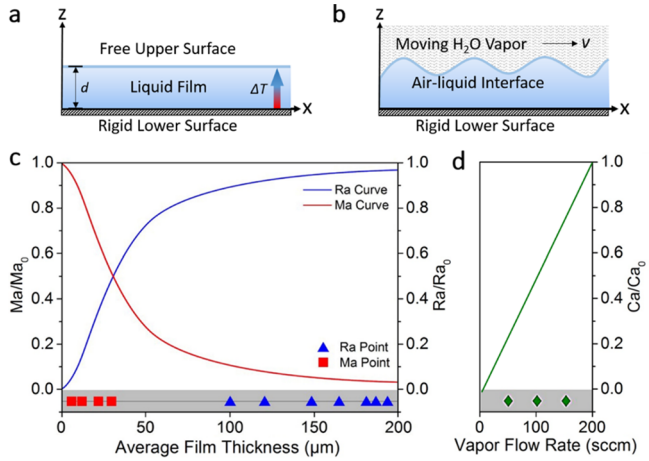

Figure 2. (a) Initial stationary state of the thin liquid film used in the coupled Rayleigh/Marangoni analysis. (b) Interfacial state of a liquid film under H_2O vapor flow. (c) Relationship between the critical dimensionless numbers and average film thickness with the marked points below classified into Ra and Ma being the film thicknesses adopted in the experiments. (d) Relationship between the H_2O vapor flow rate and capillary number ratio and the experimentally vapor flow rates marked below.

the coupled Rayleigh/Marangoni instability case, one limiting case, Ma = 0, is referred to as Rayleigh instability and the other limiting case, Ra = 0, as Marangoni instability. When stability changes, the dimensionless numbers are referred to as the critical values. The ratios of the critical dimensional numbers in the coupled and single Rayleigh/Marangoni instabilities, Ra/Ra_0 and Ma/Ma_0, are used to characterize the magnitude of a single effect in a coupled Rayleigh/Marangoni case with the following relationship[39]

$$\frac{\mathrm{Ma}(\varepsilon)}{\mathrm{Ma}_0(\varepsilon)} = 1 - \left(\frac{\mathrm{Ra}(\varepsilon)}{\mathrm{Ra}_0(\varepsilon)}\right)^{1.055} \quad (1)$$

where ε is the slope of the viscosity temperature relationship. These two ratios of the critical dimensionless numbers provide a measurement of the instability controlled mechanism. Their dependence on average film thickness d (Figure 2c) shows the transition from the buoyancy-dominated Rayleigh instability to

DOI: 10.1021/acsnano.5b05936
ACS Nano XXXX, XXX, XXX–XXX

the surface tension dominated Marangoni instability. When the thickness d is decreased, Marangoni convection becomes stronger and Rayleigh convection weakens. Therefore, the liquid thickness can be used as a controlling factor concerning the dominant effect in the dewetting process of the FF/HFIP solution. When the interfacial viscosity difference becomes significant during H_2O vapor flow over the FF/HFIP solution film (Figure 2b), the capillary number (Ca) is introduced to represent the relative effects of the viscous forces acting across the air−liquid interface. The definition is listed in Table S1. Since a flow rate exceeding 200 sccm produces a flat FF film without a unique structure, the ratio of flow rates at velocity V and 200 sccm (Ca_0) is utilized to determine the relative strength of the interfacial viscous force. This ratio Ca/Ca_0 is proportional to the characteristic velocity V of H_2O vapor when the dynamic viscosity μ and interface tension γ' are assumed to be constant at a constant temperature. Therefore, the H_2O vapor flow rate can be utilized to control the viscous fingering effect.

In the FF/HFIP solvent, Rayleigh convection dominates at a solvent film thickness of 100−250 μm and Marangoni convection at about 5−20 μm. The experimental results displayed in Figure 2c can be classified into Rayleigh convection dominant and Marangoni convection dominant. The distributions are consistent with the ratios of the critical dimensionless numbers. A larger film thickness can be achieved by mixing water with HFIP at a ratio of 1:4. If a smaller film thickness is needed, water may be omitted from the water/HFIP solvent. The water/HFIP solution is then decomposed into hundreds-of-micrometer-scale discrete droplets during evaporation in which Rayleigh convection takes place.[40] The thinner pure HFIP solvent film ruptures into polygonal parts arranged as shown by the Voronoi diagram (Figure 1d) in which Marangoni convection takes place. Water vapor also flows on the surface of a thin HFIP film deposited on an inclined substrate, and the flow rates are shown in Figure 2d. The viscosity difference between water vapor and HFIP liquid gives rise to fingering of the liquid film front in which the FF structures further develop under the capillary force. The assembled FF structures with different features that have been reported are reproduced by exploiting the different fluid mechanical effects as the solvent evaporates.

Rayleigh Convection Effect. A 100 μL portion of 3.5 mg/mL FF-dissolved HFIP/water solution (20% H_2O/80% HFIP, v/v) was laid on an FTO substrate to form droplets with enough room for Rayleigh convection. The round droplets with a radius r_1 of 50−300 μm and height h_1 of 30−100 μm (Figure 3a) decompose after the solution film evaporates at room temperature. On the basis of our calculations, the opposite upward buoyancy force and downward gravity force determine the streamline distribution consisting of a vertical flow in the center and converged flow on the bottom. The isothermal contour diagrams in Figure 3b demonstrate the evolution of the heat distribution in a single droplet with surface-bottom temperature differences of 0.05, 0.1, 1.0, 5.0, and 10 °C (from left to right). When the temperature difference is increased to 10 °C, strong vertical convection flow induces the formation of a bunch of densely aligned fibers (Figure 3c). It is very similar to that of vertical FF nanotubes shown in Figure 1c. As shown in Figure 3d, the FF fibers in the rim of a droplet are pushed away from the substrate. The enlarged image of the center knot in the inset shows that these fibers integrate into a single structure rather than loose stacks above each other. In

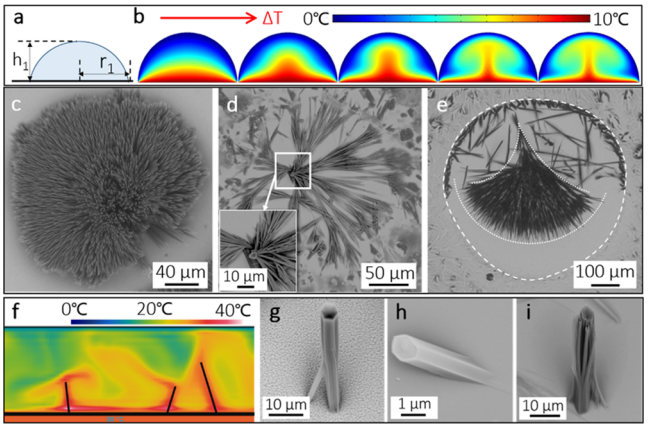

Figure 3. (a) Typical droplet dominated by Rayleigh convection with an estimated thickness h_1 of 30−100 μm and radius r_1 of 500−300 μm. (b) Simulated isothermal contour diagrams for temperature differences of 0.05, 0.1, 1.0, 5.0, and 10 °C (from left to right). (c−e) SEM analysis on the FF self-assembled structures in droplets with temperature difference ΔT of (c) 10, (d) 1, (e) 0.1 °C. The inset in panel (d) shows the knotlike FF fibers pushed upward. (f) Simulation of turbulence in the solution with a temperature difference of 30 °C. The black solid lines indicate the existence of heat plumes. (g−i) SEM images of the discrete FF structures grown from the heat plumes with (g) vertical hexagonal FF nanotube, (h) inclined hexagonal FF nanorod, and (i) vertical FF nanorod assembled by the filament bundle.

the distorted droplet caused by disturbing the external environment, only a part of the bottom is filled with the dispersive FF fibers and others are full of disordered tubes and rods (Figure 3e). The arrangement corresponds to the streamline distribution in our simulation.[41,42] Further simulation of the turbulent situation (Figure 3f) demonstrates that the nonuniform plumes rising from the substrate result in the formation of randomly arranged FF rods and tubes (Figure 3g−i). They adhere to the substrate and are oriented randomly. Most of them possess a hexagonal shape (Figure 3g,h), and some contain fine filaments aligned along the longitudinal axis (Figure 3i). These filaments are assembled in the flowing stream and adhere to each other as driven by surface hydrophobicity and terminal electrostatic force.[2,43] Ostwald ripening facilitates the formation of the regular hexagonal tubes.[44] Other examples of discrete FF rods and tubes randomly arranged in a turbulent droplet are illustrated in Figure S1. These discrete hexagonal tubes/rods in Figure 3g−i grow from the heat plumes which appear in turbulent Rayleigh convection. The plumes stem from the irregular heat distribution of the bottom and are not related to a single convection cell (see Figure S1a). The diameter of the tube is hard to control because changes in the external environment cannot accurately affect the internal chaotic convective flow. The correlation between convective stream distribution and morphology of the FF structures supports attempts to control FF self-assembly by changing the solution environment.[32]

Marangoni Convection Effect. A 50−200 μL portion of the FF/HFIP solution were laid on the FTO substrate. The oil-like HFIP solvent expanded on the surface to form a thin liquid film with a thickness h_2 of 5−20 μm. The film was left in a chamber full of water vapor to evaporate at different temperatures.[2] The Voronoi diagram shows the adjoining polygonal films formed by rupturing (Figure 4e). According to our simulation,[35] the stream flowing from the center to rim

DOI: 10.1021/acsnano.5b05936
ACS Nano XXXX, XXX, XXX−XXX

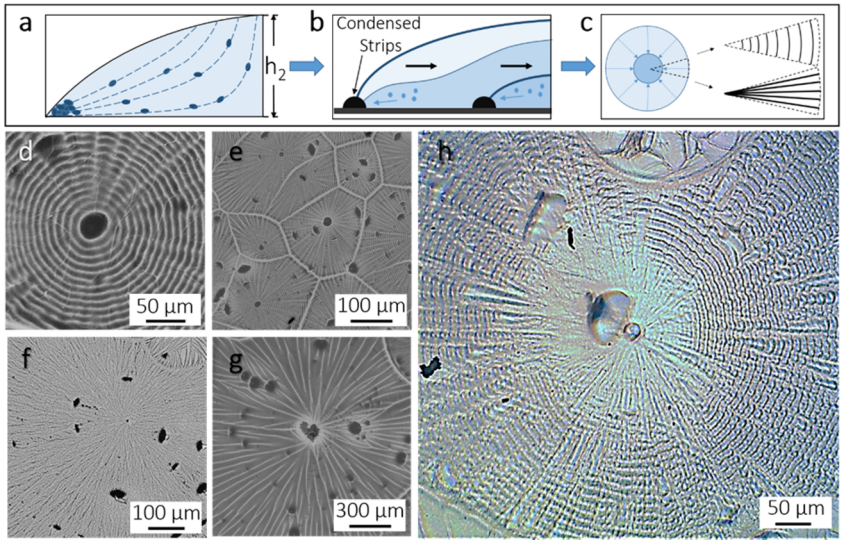

Figure 4. (a–c) Proposed mechanism for pattern formation induced by Marangoni convection. (a) FF monomers gather along the streamlines to form structures at the rim of liquid film with an average height h_2 of 5–20 μm. (b) Periodic strips form by the proposed "stick–slip" mechanism. (c) Two kinds of patterns form when the liquid film shrinks: concentric (up) and spokelike (down). (d) SEM image of a single concentric pattern. (e) General view of several concentric patterns joined together like a Voronoi diagram. (f, g) SEM images of the spokelike patterns produced at FF concentrations: (f) 1 and (g) 3 mg/mL. (h) Optical image of the pattern consisting of both radially arranged bumps and concentrically surrounded strips.

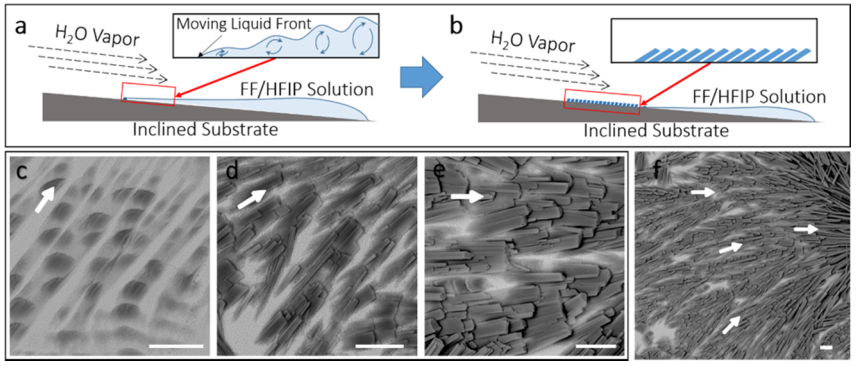

Figure 5. (a, b) Schematics of the experimental processes to produce flakelike FF structures on a tilt. (a) FF/HFIP solution is deposited on an inclined substrate and H_2O vapor flows over the liquid surface. Inset: Convective flow near the moving liquid front. (b) Inclined flakes form on the area where liquid front passes by. (c–e) SEM images of the inclined flakes formed under different water vapor flow rates: (c) 150, (d) 100, and (e) 50 sccm. (f) General view of the grown flakes. The white arrows indicate directions to which the liquid front moves. Scale bars: 10 μm.

would appear under Marangoni stress (Figure 4a). The components for self-assembly are guided along the streamlines to gather on the rim of the droplets forming circular belts (Figure S2a,b),[45] and then the "stick–slip" mechanism takes place as the film shrinks and circular contact lines contract (Figure 4b).[46,47] The pinning force arising from the interface tension between the condensed belts and solution nearby suspends the shrinking liquid film. As evaporation occurs, the contracting tendency becomes stronger until the pinning force cannot hold it anymore. The liquid film with a smaller volume forms a smaller circle on the rim, which forms a new belt. Hence, concentric belts appear after the liquid film evaporates completely. Condensation on the rim takes a relatively long time to form the enclosed belts. If the evaporation rate is large, spokelike lines are observed instead of concentric belts due to the large contracting rate and short deposition time (Figure 4c). According to our experiments, the concentric patterns (Figure 4d,e and Figure S2c,d) usually form at around 10 °C, and the spokelike patterns form (Figure 4f,g) at around 30 °C. At a medium temperature of 15–25 °C, a hybrid pattern consisting of both radially arranged bumps and concentrically surrounded strips appears (Figure 4h and Figure S2e,f). It may be designated as the intermediate state of concentric and spokelike patterns. Production of the periodic pattern with high symmetry indicates that FF can be used in pattern construction on a two-dimensional surface by controlling the solution and environment, thereby providing a viable method for large-scale surface patterning of peptides.[48]

Viscous Fingering Effect. A 200 μL portion of 4 mg/mL FF/HFIP were laid on a 5° inclined FTO substrate. The reason for the tilt is that the liquid film formed on a flat plane usually ruptures irregularly.[36,37,49] On an inclined substrate, most of the film can preserve the integrity when the liquid front moves downward because the solution in the thicker bottom keeps supplementing the loss of the thinner top during evaporation. After deposition of the solution, H_2O vapor flow produced by passing nitrogen gas through pure water is applied to the upper surface of the liquid film (Figure 5a). A vortex is formed in the

DOI: 10.1021/acsnano.5b05936
ACS Nano XXXX, XXX, XXX–XXX

thin liquid film due to the viscosity difference between air and HFIP solution (inset, Figure 5a). Viscous fingering on the upper rim enables the liquid front to split into parallel lines, and in these aligned solution fingers, flakes grow from the substrate by FF self-assembly (Figure 5b).[50,51] At a high air flow velocity (150 sccm), the liquid front moves quickly during evaporation and only small slices form on the substrate (Figure 5c). As the air flow becomes slower, more time is left for the structure formation before the film becomes completely dry and viscous forces also become weaker. Long and bulky architectures are produced when the flow rate is reduced to 100 (Figure 5d) and 50 sccm (Figure 5e). Figure 5f and Figure S3 illustrate that the flakes grow toward the direction along which the liquid front moves, thus enabling control of the spatial organization of the nanostructures.

The functionality of the self-assembled FF architectures is related to the molecular arrangement and lattice structures.[2,9,26] Despite the porous FF nanostructures, the interpenetrating "zipper-like" aromatic rings interlock to form an array of rigid nanotube backbones with unexpected stiffness and robustness.[9] To investigate the dominance of the various effects on the molecular structure of the self-assembled architecture, XRD and Raman spectra are acquired from the three FF nanostructures shown in the SEM images in Figures 3d, 4e, and 5f. The XRD results are presented in Figure S4 and for comparison, and the results obtained from the interconnected hexagonal microtubes are also shown (inset). XRD suggests that all of the self-assembled FF architectures possess a molecular structure similar to those reported previously.[22,52,53] The Raman spectra also suggest the same conclusion (Figure S5), implying that controlled FF self-assembly in dewetting solutions does not change the lattice structure significantly.

CONCLUSION

Three experiments were designed and performed to study whether Rayleigh convection, Marangoni convection, and vicious fingering are dominant in FF self-assembly and structure formation based on stimulation of the evaporative dewetting processes of FF-dissolved solution. Rayleigh convection in water/HFIP droplets guides the formation of converged fibers in a steady environment, and discrete tubes and rods are formed under turbulent conditions. Both are related to the convective streamline distribution. Marangoni convection in a thin liquid film induces a centrosymmetric pattern formation by the "stick−slip" mechanism. The patterns further evolve into spokelike or concentric patterns by controlling the evaporation rate which changes with temperature. Viscous fingering arising from viscosity difference in the phase boundary of water vapor and HFIP solution produces adjoining microrods oriented toward the direction in which the liquid front moves on the inclined substrate. XRD and Raman scattering indicate that all the self-assembled architectures possess the same structure. The results suggest a simple and convenient strategy to produce complicated self-assembled structure on a large scale by controlling the dewetting process of peptides in the liquid environment.

METHODS

Materials. The lyophilized form of FF was purchased from Bachem (Bubendorf, Switzerland), and 1,1,1,3,3,3-hexafluoro-2-propanol (HFIP) was purchased from Aladdin (Shanghai, China). Deionized water (18.2 MΩ/cm) used in the experiments was produced by a Millipore nanopure water system, and the FTO glass was purchased from Nanjing Chemical Reagent Co., Ltd. (Nanjing, China).

Preparation of FF Structures. The experiments were performed in cylindrical chambers. Slides serving as substrates were washed with pure water and acetone three times and dried. The water vapor was formed by putting a fixed volume of pure water inside the chamber and then heating to 22 °C for 6 h. The FF solution was prepared fresh to avoid aggregation by dissolving the as-received FF powders in the HFIP by sonication.

Characterization. Optical microscopy was carried out on a Nikon Eclipse 80i (Nikon, Japan). The samples were coated with a 10 nm thick gold layer prior to SEM examination on the Phenom ProX (Phenom-World, The Netherlands). The crystalline structure was determined on a Philips Xpert diffractometer and Raman scattering spectra were acquired on a T64000 triple Raman system (HORIBA Scientific, USA). The film thickness was estimated on the Zeta 20 (Zeta Instruments, USA).

Simulation. The simulation in Figure 3b was performed using COMSOL Multiphysics 5.0 software (COMSOL Inc., Stockholm, Sweden), and that in Figure 3f was conducted using Energy2D software.[54]

ASSOCIATED CONTENT

Supporting Information

The Supporting Information is available free of charge on the ACS Publications website at DOI: 10.1021/acsnano.5b05936.

Table S1: definition of some parameters. Figures S1−S5: SEM images, optical images, XRD spectra, and Raman spectra (PDF)

AUTHOR INFORMATION

Corresponding Author

*E-mail: hkxlwu@nju.edu.cn. Fax: 86-25-83595535. Tel: 86-25-83686303.

Notes

The authors declare no competing financial interest.

ACKNOWLEDGMENTS

This work was supported by the National Basic Research Programs of China under Grant Nos. 2013CB932901 and 2014CB339800 and the National Natural Science Foundation (Nos. 11374141 and 61521001), City University of Hong Kong Applied Research Grant (ARG) No. 9667104, and City University of Hong Kong Strategic Research Grant (SRG) No. 7004188.

REFERENCES

(1) Reches, M.; Gazit, E. Casting Metal Nanowires within Discrete Self-Assembled Peptide Nanotubes. *Science* **2003**, *300*, 625−627.

(2) Wang, M. J.; Du, L. J.; Wu, X. L.; Xiong, S. J.; Chu, P. K. Charged Diphenylalanine Nanotubes and Controlled Hierarchical Self-Assembly. *ACS Nano* **2011**, *5*, 4448−4454.

(3) Yan, X. H.; Zhu, P. L.; Li, J. B. Self-Assembly and Application of Diphenylalanine -Based Nanostructures. *Chem. Soc. Rev.* **2010**, *39*, 1877−1890.

(4) Gazit, E. Self-Assembled Peptide Nanostructures: the Design of Molecular Building Blocks and their Technological Utilization. *Chem. Soc. Rev.* **2007**, *36*, 1263−1269.

(5) Zhang, J. L.; Wu, X. L.; Gan, Z. X.; Zhu, X. B.; Jin, Y. M. Unidirectionally Aligned Diphenylalanine Nanotube/Microtube Arrays with Excellent Supercapacitive Performance. *Nano Res.* **2014**, *7*, 929−937.

(6) Yemini, M.; Reches, M.; Gazit, E.; Rishpon, J. Peptide Nanotube-Modified Electrodes for Enzyme-Biosensor Applications. *Anal. Chem.* **2005**, *77*, 5155−5159.

DOI: 10.1021/acsnano.5b05936
ACS Nano XXXX, XXX, XXX−XXX

(7) Cipriano, T. C.; Takahashi, P. M.; De Lima, D.; Oliveira, V. X.; Souza, J. A.; Martinho, H.; Alves, W. A. Spatial Organization of Peptide Nanotubes for Electrochemical Devices. *J. Mater. Sci.* **2010**, *45*, 5101−5108.
(8) Ryu, J.; Lim, S.; Park, C. Photoluminescent Peptide Nanotubes. *Adv. Mater.* **2009**, *21*, 1577−1581.
(9) Azuri, I.; Adler-Abramovich, L.; Gazit, E.; Hod, O.; Kronik, L. Why Are Diphenylalanine-Based Peptide Nanostructures so Rigid? Insights from First Principles Calculations. *J. Am. Chem. Soc.* **2014**, *136*, 963−969.
(10) Guo, C.; Luo, Y.; Zhou, R. H.; Wei, G. H. Probing the Self-Assembly Mechanism of Diphenylalanine-Based Peptide Nanovesicles and Nanotubes. *ACS Nano* **2012**, *6*, 3907−3918.
(11) Rissanou, A. N.; Georgilis, E.; Kasotakis, E.; Mitraki, A.; Harmandaris, V. Effect of Solvent on the Self-Assembly of Dialanine and Diphenylalanine Peptides. *J. Phys. Chem. B* **2013**, *117*, 3962−3975.
(12) Jeon, J.; Mills, C. E.; Shell, S. M. Molecular Insights into Diphenylalanine Nanotube Assembly: All-Atom Simulations of Oligomerization. *J. Phys. Chem. B* **2013**, *117*, 3935−3943.
(13) Jeon, J.; Shell, M. S. Self-Assembly of Cyclo-Diphenylalanine Peptides in Vacuum. *J. Phys. Chem. B* **2014**, *118*, 6644−6652.
(14) Berne, B. J.; Weeks, J. D.; Zhou, R. H. Dewetting and Hydrophobic Interaction in Physical and Biological Systems. *Annu. Rev. Phys. Chem.* **2009**, *60*, 85−103.
(15) Reiter, G. Unstable Thin Polymer-Films-Rupture and Dewetting Processes. *Langmuir* **1993**, *9*, 1344−1351.
(16) Deegan, R. D.; Bakajin, O.; Dupont, T. F.; Huber, G.; Nagel, S. R.; Witten, T. A. Capillary Flow as the Cause of Ring Stains from Dried Liquid Drops. *Nature* **1997**, *389*, 827−829.
(17) Han, W.; Lin, Z. Q. Learning from "Coffee Rings": Ordered Structures Enabled by Controlled Evaporative Self-Assembly. *Angew. Chem., Int. Ed.* **2012**, *51*, 1534−1546.
(18) Neogi, P. Tears-of-Wine and Related Phenomena. *J. Colloid Interface Sci.* **1985**, *105*, 94−101.
(19) Cai, Y. J.; Newby, B. Z. Marangoni Flow-Induced Self-Assembly of Hexagonal and Stripelike Nanoparticle Patterns. *J. Am. Chem. Soc.* **2008**, *130*, 6076−6077.
(20) Maillard, M.; Motte, L.; Pileni, M. Rings and Hexagons Made of Nanocrystals. *Adv. Mater.* **2001**, *13*, 200−204.
(21) Rabani, E.; Reichman, D. R.; Geissler, P. L.; Brus, L. E. Drying-Mediated Self-Assembly of Nanoparticles. *Nature* **2003**, *426*, 271−274.
(22) Li, Q.; Jia, Y.; Dai, L. R.; Yang, Y.; Li, J. B. Controlled Rod Nanostructured Assembly of Diphenylalanine and their Optical Waveguide Properties. *ACS Nano* **2015**, *9*, 2689−2695.
(23) Reches, M.; Gazit, E. Controlled Patterning of Aligned Self-Assembled Peptide Nanotubes. *Nat. Nanotechnol.* **2006**, *1*, 195−200.
(24) Hendler, N.; Sidelman, N.; Reches, M.; Gazit, E.; Rosenberg, Y.; Richter, S. Formation of Well-Organized Self-Assembled Films from Peptide Nanotubes. *Adv. Mater.* **2007**, *19*, 1485−1488.
(25) Ryu, J.; Park, C. B. Solid-Phase Growth of Nanostructures from Amorphous Peptide Thin Film: Effect of Water Activity and Temperature. *Chem. Mater.* **2008**, *20*, 4284−4290.
(26) Gan, Z. X.; Wu, X. L.; Zhu, X. B.; Shen, J. C. Light-Induced Ferroelectricity in Bioinspired Self-Assembled Diphenylalanine Nanotubes/Microtubes. *Angew. Chem.* **2013**, *125*, 2109−2113.
(27) Vasudev, M. C.; Koerner, H.; Singh, K. M.; Partlow, B. P.; Kaplan, D. L.; Gazit, E.; Bunning, T. J.; Naik, R. R. Vertically Aligned Peptide Nanostructures Using Plasma-Enhanced Chemical Vapor Deposition. *Biomacromolecules* **2014**, *15*, 533−540.
(28) Kim, J.; Han, T.; Kim, Y.; Park, J.; Choi, J.; Churchill, D. G.; Kim, S.; Ihee, H. Role of Water in Directing Diphenylalanine Assembly into Nanotubes and Nanowires. *Adv. Mater.* **2010**, *22*, 583−587.
(29) Lee, J. S.; Yoon, I.; Kim, J.; Ihee, H.; Kim, B.; Park, C. B. Self-Assembly of Semiconducting Photoluminescent Peptide Nanowires in the Vapor Phase. *Angew. Chem.* **2011**, *123*, 1196−1199.
(30) Sedman, V. L.; Adler-Abramovich, L.; Allen, S.; Gazit, E.; Tendler, S. J. B. Direct Observation of the Release of Phenylalanine from Diphenylalanine Nanotubes. *J. Am. Chem. Soc.* **2006**, *128*, 6903−6908.
(31) Martins, T. D.; De Souza, M. I.; Cunha, B. B.; Takahashi, P. M.; Ferreira, F. F.; Souza, J. A.; Fileti, E. E.; Alves, W. A. Influence of PH and Pyrenyl on the Structural and Morphological Control of Peptide Nanotubes. *J. Phys. Chem. C* **2011**, *115*, 7906−7913.
(32) Mason, T. O.; Chirgadze, D. Y.; Levin, A.; Adler-Abramovich, L.; Gazit, E.; Knowles, T. P. J.; Buell, A. K. Expanding the Solvent Chemical Space for Self-Assembly of Dipeptide Nanostructures. *ACS Nano* **2014**, *8*, 1243−1253.
(33) Wang, Y. F.; Huang, R. L.; Qi, W.; Xie, Y. Y.; Wang, M. F.; Su, R. X.; He, Z. M. Capillary Force-Driven, Hierarchical Co-Assembly of Dandelion-Like Peptide Microstructures. *Small* **2015**, *11*, 2893−2902.
(34) Ahlers, G.; Grossmann, G. A. S.; Lohse, D. Heat Transfer and Large Scale Dynamics in Turbulent Rayleigh-Bénard Convection. *Rev. Mod. Phys.* **2009**, *81*, 503−537.
(35) Sempels, W.; De Dier, R.; Mizuno, H.; Hofkens, J.; Vermant, J. Auto-Production of Biosurfactants Reverses the Coffee Ring Effect in a Bacterial System. *Nat. Commun.* **2013**, *4*, 1757.
(36) Álvarez-Lacalle, E.; Ortín, J.; Casademunt, J. Relevance of Dynamic Wetting in Viscous Fingering Patterns. *Phys. Rev. E* **2006**, *74*, 79−97.
(37) Oron, A.; Davis, S.; Bankoff, S. Long-Scale Evolution of Thin Liquid Films. *Rev. Mod. Phys.* **1997**, *69*, 931−980.
(38) Cross, M. C.; Hohenberg, P. C. Pattern-Formation outside of Equilibrium. *Rev. Mod. Phys.* **1993**, *65*, 851−1112.
(39) Skarda, J. R. L.; Mccaughan, F. E. Coupled Marangoni-Benard/Rayleigh-Benard Instability with Temperature Dependent Viscosity. *NASA STI/Recon Tech. Rep.* **1994**, *94*, 106646.
(40) Bestehorn, M.; Merkt, D. Regular Surface Patterns on Rayleigh-Taylor Unstable Evaporating Films Heated from Below. *Phys. Rev. Lett.* **2006**, *97*, 127802−128110.
(41) Basu, A. S.; Gianchandani, Y. B. Shaping High-Speed Marangoni Flow in Liquid Films by Microscale Perturbations in Surface Temperature. *Appl. Phys. Lett.* **2007**, *90*, 034102.
(42) Sáenz, P. J.; Sefiane, K.; Kim, J.; Matar, O. K.; Valluri, P. Evaporation of Sessile Drops: a Three-Dimensional Approach. *J. Fluid Mech.* **2015**, *772*, 705−739.
(43) Reches, M.; Gazit, E. Molecular Self-Assembly of Peptide Nanostructures: Mechanism of Association and Potential Uses. *Curr. Nanosci.* **2006**, *2*, 105−111.
(44) Levin, A.; Mason, T. O.; Adler-Abramovich, L.; Buell, A. K.; Meisl, G.; Galvagnion, C.; Bram, Y.; Stratford, S. A.; Dobson, C. M.; Knowles, T. P. J.; Gazit, E. Ostwald's Rule of Stages Governs Structural Transitions and Morphology of Dipeptide Supramolecular Polymers. *Nat. Commun.* **2014**, *5*, 5219.
(45) Hong, S.; Xia, J.; Lin, Z. Spontaneous Formation of Mesoscale Polymer Patterns in an Evaporating Bound Solution. *Adv. Mater.* **2007**, *19*, 1413−1417.
(46) Bodiguel, H.; Doumenc, F.; Guerrier, B. Stick-Slip Patterning at Low Capillary Numbers for an Evaporating Colloidal Suspension. *Langmuir* **2010**, *26*, 10758−10763.
(47) Sandnes, B.; Flekkøy, E.; Knudsen, H.; Maløy, K.; See, H. Patterns and Flow in Frictional Fluid Dynamics. *Nat. Commun.* **2011**, *2*, 388.
(48) Huang, J. X.; Kim, F.; Tao, A. R.; Connor, S.; Yang, P. D. Spontaneous Formation of Nanoparticle Stripe Patterns through Dewetting. *Nat. Mater.* **2005**, *4*, 896−900.
(49) Seemann, R.; Herminghaus, S.; Jacobs, K. Dewetting Patterns and Molecular Forces: a Reconciliation. *Phys. Rev. Lett.* **2001**, *86*, 5534−5537.
(50) De Wit, A.; Eckert, K.; Kalliadasis, S. Introduction to the Focus Issue: Chemo-Hydrodynamic Patterns and Instabilities. *Chaos* **2012**, *22*, 037101.
(51) Mavromoustaki, A.; Bertozzi, A. L. Hyperbolic Systems of Conservation Laws in Gravity-Driven, Particle-Laden Thin-Film Flows. *J. Eng. Math.* **2014**, *88*, 29.
(52) Górbitz, C. The Structure of Nanotubes Formed by Diphenylalanine, the Core Recognition Motif of Alzheimer's β-Amyloid Polypeptide. *Chem. Commun.* **2006**, *22*, 2332−2334.

DOI: 10.1021/acsnano.5b05936
ACS Nano XXXX, XXX, XXX−XXX

(53) Wu, X. L.; Xiong, S. J.; Wang, M. J.; Shen, J. C.; Chu, P. K. Low-Frequency Raman Scattering of Bioinspired Self-Assembled Diphenylalanine Nanotubes/Microtubes. *Opt. Express* **2012**, *20*, 5119−5126.
(54) Xie, C. Interactive Heat Transfer Simulations for Everyone. *Phys. Teach.* **2012**, *50*, 237−241.

DOI: 10.1021/acsnano.5b05936
ACS Nano XXXX, XXX, XXX−XXX